nature nanotechnology

SUPPLEMENTARY INFORMATION

DOI: 10.1038/NNANO.2011.3

Supplementary Information: Gate-controlled guiding of electrons in graphene

J. R. Williams,[1,*] Tony Low,[2] M. S. Lundstrom,[2] and C. M. Marcus[3]

[1]*School of Engineering and Applied Sciences, Harvard University, Cambridge, MA 02138, USA*
[2]*School of Electrical & Computer Engineering, Purdue University, West Lafayette, IN 47906, USA*
[3]*Department of Physics, Harvard University, Cambridge, MA 02138, USA*

(Dated: December 25, 2010)

I. Landauer-Büttiker and transport coefficients

Two measurement geometries were employed, the "channel" and "focusing" geometries. Measurements of the three resistances R_{ii}, R^f_{ii} and R^f_{ic} are shown in Fig. S1 as a function of top gate voltage $V_{\rm tg}$. Contact i is connected to a current source of I_i, and c is connected to ground or a voltmeter for the "channel" and "focusing" geometry respectively. The following resistances were then measured,

$$R_{ii} = V_{ig}/I_i \;\;,\;\; R^f_{ii} = V_{ig}/I_i \;\;,\;\; R^f_{ic} = V_{cg}/I_i. \qquad (1)$$

From these resistances, one can relate them to transport coefficiencts such as transmission function $\mathcal{T}_{ij}$ and Ω through the Landauer-Büttiker equation. The Landauer-Büttiker equation for the "channel" geometry at contact i is simply given by,

$$R_q I_i = \mathcal{T}_{ii}\mu_i \Rightarrow R_{ii} = R_q \mathcal{T}_{ii}^{-1} \qquad (2)$$

where R_q is the quantum resistance and $\mathcal{T}_{ii} = \mathcal{T}_{ic} + \mathcal{T}_{ig1} + \mathcal{T}_{ig2}$. From Eq. 2, one expects $R_{ii}(ppp) < R_{ii}(pnp)$, since $\mathcal{T}_{ii}(ppp) > \mathcal{T}_{ii}(pnp)$. This is consistent with experiments (see Fig. S1). In similar fashion, we write for "focusing" geometry at contact i,

$$R_q I_i = \mathcal{T}_{ii}\mu_i - \mathcal{T}_{ci}\mu_c. \qquad (3)$$

Combining Eq. 2 and 3 one arrives at,

$$R^f_{ii} = R_{ii} + \mathcal{T}_{ci}\mathcal{T}_{ii}^{-1} R^f_{ic} > R_{ii}. \qquad (4)$$

We note that the inequality expressed by Eq. 4 is consistent with experimental observation (Fig. S1). The inequality in Eq. 4 implies that Ω_{exp} increases with the difference in chemical potentials, i.e. $\mu^f_i - \mu_i$, between the two geometries. Conversely, it means that if the guiding is negligible, then attaching a voltage probe at c would not impact the chemical potential at i i.e. $\mu^f_i \approx \mu_i$. However, one could also write the Landauer-Büttiker equation for contact c instead. This would give the more familiar form originally used for the "focusing" geometry in Ref. [1],

$$R^f_{ic} = \mathcal{T}_{cc}^{-1}\mathcal{T}_{ic} R^f_{ii} < R^f_{ii}. \qquad (5)$$

The inequality expressed by Eq. 5 is consistent with our experiments (Fig. S1). The inequality in Eq. 5 implies

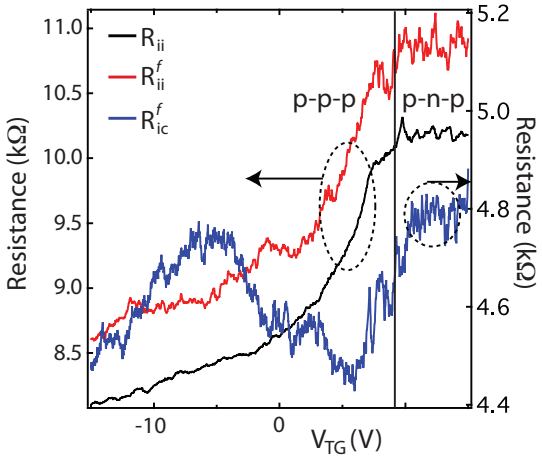

FIG. S1: The three experimentally obtained resistances R_{ii}, R^f_{ii} and R^f_{ic} as a function of the top gate voltage $V_{\rm tg}$.

that Ω_{exp} decreases with the difference in chemical potentials, i.e. $\mu^f_i - \mu^f_c$, in the focusing geometry. Conversely, it means that if the guiding is perfect, then terminal i and c are electrically shorted i.e. $\mu^f_i \approx \mu^f_c$

As stated in the main text, a quantitative estimation of the experimental guiding efficiency is obtained by taking the average of $\Omega_{exp} = \mathcal{T}_{ci}/\mathcal{T}_{ii}$ and $\Omega_{exp} = \mathcal{T}_{ic}/\mathcal{T}_{cc}$ from Eq. 4 and Eq. 5 respectively,

$$\Omega_{exp} \approx \frac{1}{2}\left[\frac{R^f_{ii} - R_{ii}}{R^f_{ic}} + \frac{R^f_{ic}}{R^f_{ii}}\right] \qquad (6)$$

Eq. 6 is what we employ in the main paper when comparing with numerical simulations. For qualitative purposes, one could also similarly employ Eq. 5 instead, and similar conclusions as discussed in the paper would also be reached.

In graphene, it is known that placement of metal contacts can dope the graphene underneath [2]. The p-n interface formed would lead to a smaller $\mathcal{T}_{ii}$ than it would have been otherwise, which is already captured in the measurement of R_{ii}.

DOI: 10.1038/NNANO.2011.3

IIa. Quantum transport: numerics

Here, we give a brief description of the numerics and transport model. A Hamiltonian for graphene within the nearest-neighbor p_z-orbital tight binding model [5] is used,

$$\mathcal{H} = \sum_i v_i a_i^\dagger a_i + \sum_{ij} |t_{ij}|\, exp\left(i\frac{q}{\hbar}\int_i^j \mathbf{A}\cdot d\mathbf{l}\right) a_i^\dagger a_j, \quad (7)$$

where $a_i^\dagger/a_i$ are the creation/destruction operator at each atomic site i. v_i is the on-site potential energy, controlled by $V_{\rm tg}$ and $V_{\rm bg}$. $|t_{ij}|$ is the p_z-orbital hopping energy, set to 3 eV. In the presence of a perpendicular magnetic field B, t_{ij} contains a Peierls phase, where $\mathbf{A}$ is the vector potential. The central quantity of the quantum transport theory, the retarded Green function $\mathcal{G}$ is written as (see [6, 7] for general theory),

$$\mathcal{G} = [(\epsilon_f + i\eta)\mathcal{I} - \mathcal{H} - \mathcal{V} - \Sigma]^{-1} \quad (8)$$

where ϵ_f is the Fermi energy and Σ is the sum of all contact self energies i.e. Σ_i, Σ_c, Σ_{g1} and Σ_{g2}. Σ_j can be obtained once the contacts' surface Green function, g_j, is calculated. In this work, we compute g_j iteratively using the algorithm described in Ref. [8], based on the decimation technique (see e.g. [9]). Finally, the energy-resolved current through contact n due to an injection from contact m can be obtained through [6, 7],

$$\mathcal{I}_n(\epsilon) = \frac{2q^2}{h} Tr\left[\Sigma_n^{in}(\epsilon)\mathcal{A}(\epsilon) - \Gamma_n(\epsilon)\mathcal{G}^n(\epsilon)\right] \quad (9)$$

where $\mathcal{A}{=}i(\mathcal{G} - \mathcal{G}^\dagger)$ is the local density-of-states, $\Sigma_j^{in}{=}f_j(\epsilon)\Gamma_j(\epsilon)$ is the filling function (analogous to the in-scattering function for incoherent case), $f_j(\epsilon)$ is the Fermi function of contact j, and $\Gamma_j{=}i(\Sigma_j{-}\Sigma_j^\dagger)$ is the contact broadening function. In Eq. 9, $\mathcal{G}^n(\epsilon)$ is the electron correlation function given by $\mathcal{G}\Sigma^{in}\mathcal{G}^\dagger$. To compute the current due to injection from contact m, we set $f_m = 1$ and $f_{j\neq m} = 0$. The transmission function from contact m to n is given by $\mathcal{T}_{mn} = \frac{h}{2q^2}\mathcal{I}_n/(f_m - f_n)$.

Usually, the size of the $\mathcal{G}$ matrices is too computationally prohibitive for its inverse to be sought directly. Hence, $\mathcal{G}$ and $\mathcal{G}^n$ are usually computed using techniques commonly known as the "recursive Green function algorithm" (see for example [10]) and the "renormalization method" (see for example [11]). It exploits the special properties of the tridiagonal nature of $\mathcal{H}$ through the use of Dyson's equation. We used a combination of these methods to compute the device charge and current density in a memory efficient manner, described elsewhere [4].

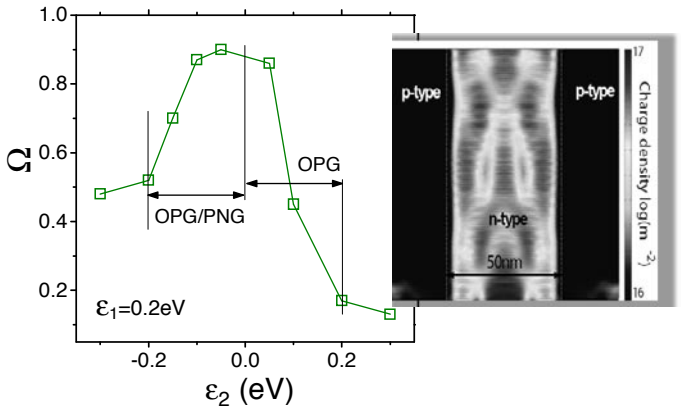

FIG. S2: Simulated Ω as a function of ϵ_2 with $\epsilon_1 = 0.2eV$. The operating regime, i.e. OPG or OPG/PNG, is illustrated. Inset: Plot of charge density of the device, for the case where $\epsilon_1 = -\epsilon_2 = 0.3eV$. See text here for more description of the device.

IIb. Quantum transport: simulations

To model the experimental device, we assumed a graphene sheet with dimensions W=L=100 nm. The contacts width for i, c are assumed to be 50 nm while that of $g1, g2$ are 100 nm. The channel width, which is controlled by the top gate, is assumed to be 50 nm. Fig. S2 inset shows the calculated non-equlibrium charge density of the device at the Fermi energy for some typical values of $\epsilon_{1,2}$, and assumed initially that the channel interfaces were perfect. In the main manuscript, we relaxed this assumption in order to explain the experimental trends and to achieve quantitative agreement with the experiments. As shown in the inset of Fig. 3 in the main manuscript, the following experimental trend was observed: $\Omega_{OPG} > \Omega_{OPG/PNG} > \Omega_{PNG}$ at a given back-gate voltage V_{bg} or ϵ_2. Fig. S2 shows the calculated Ω as a function of ϵ_2 assuming perfect interface for the channel, for ϵ_1=0.2 eV. The OPG and OPG/PNG regimes are indicated. The simulation shows that Ω_{OPG} is always smaller than its $\Omega_{OPG/PNG}$ counterpart. This is in contrary to the experimental observations.

Adding p-n interface roughness, i.e. the root mean square of the in-plane variations normal to the p-n interface, is necessary to obtain corroboration with the experimental trend, as discussed in the manuscript. P-n interface roughness is implemented according to the exponential power spectrum model (a common model used to describe 2D interface roughness) as described in Ref. [12]. These interface roughness profiles are smoothly varying over atomic length scale. In the manuscript, we simply quote the average root-mean-square of the statistical sample over dozen realizations. The impact of choice of power spectrum of the roughness on guiding efficiency is not studied in this work. Such a study is impeded by the lack of experimental knowledge and characterization work on p-n interface disorder and it is computationally

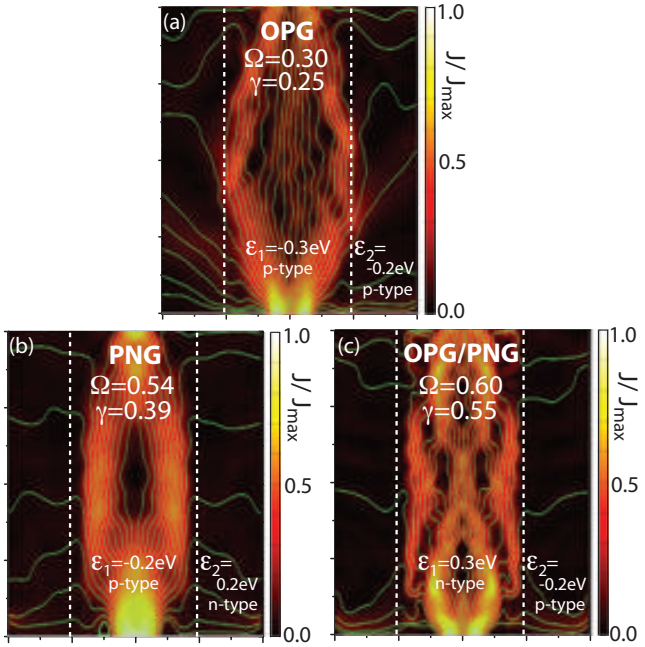

FIG. S3: Simulations of electron guiding for (a) 2 nm of interface disorder and 0 nm of interface disorder (disorder free) for the (b) PNG and (c) OPG/PNG regimes.

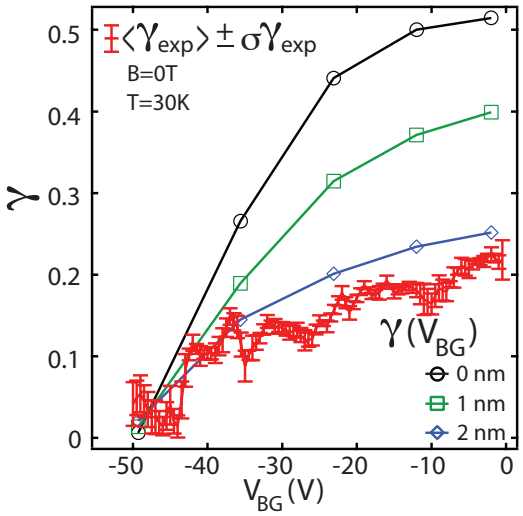

FIG. S4: The average value of the corrected guiding efficiency $\langle\gamma_{exp}\rangle$ and its standard deviation $\sigma\gamma_{exp}$ calculated for the OPG regime.

expensive to examine these large parameter spaces. However, we should emphasize that the general conclusions derived from our transport modeling in disordered regime should be fairly robust against the specific power spectrum model employed and the general trend observed – that interface disorder degrades guiding efficiency should be universal.

In the main text, we show simulations for the disorder-free case for the OPG regime and 2 nm of interface disorder for the PNG and OPG/PNG regimes. In Fig. S3, we compliment that data with the simulations for 2 nm of interface disorder in the OPG regime and the disorder-free scenario for PNG and OPG/PNG.

III. Average Value and Standard Deviation of γ_{exp} in the OPG Regime

Fluctuations in resistance with gate voltage (universal conductance fluctuations) can cause R_{ii}, R^f_{ii} and R^f_{ic} to vary. These fluctuations will cause variations in the value of Ω_{exp} and γ_{exp}. If the fluctuations are large, the ability to distinguish the various amounts of disorder (0, 1 and 2 nm in Fig. 3 of the main text) will be diminished. To quantify these fluctuations, we calculate, by averaging over the top-gate voltage in the experimental data, an average value of the corrected guiding efficiency $\langle\gamma_{exp}\rangle$ (using the "equal-epsilon" value used in the text of 0.26), and its standard deviation, $\sigma\gamma_{exp}$, as a function of back-gate voltage in Fig. S4. It is clear that the variations are small, most likely owing to the large measurement temperature (T=30K), and hence, we are able to show that 2nm, and not 0 or 1nm, is most likely the correct value to use in numerical simulations. Further, we note that the trend in back-gate voltage of $\langle\gamma_{exp}\rangle$ is similar to γ_{exp} in Fig. 3 of the main text, indicating that there is not much variation and the the one-dimensional cut of Fig. 3 is representative of the back-gate voltage dependence in the OPG regime.

* Present address: Department of Physics, Stanford University, Stanford, CA 94305, USA.

[1] van Houten, H. *et al.*, Coherent electron focusing with quantum point contacts in a two-dimensional electron gas. *Phys. Rev. B* **39**, 8556-8575 (1989).
[2] Huard, B., Stander, N., Sulpizio, J. A., Goldhaber-Gordon, D. Evidence of the role of contacts on the observed electron-hole asymmetry in graphene. *Phys. Rev. B* **78**, 121402(R) (2008).
[3] Low, T., Hong, S., Appenzeller, J., Datta, S., & Lundstrom, M. S. Conductance Asymmetry of Graphene p-n Junction. *IEEE Trans. Elec. Dev.* **56**, 1292 (2009).
[4] Low, T. & Appenzeller, J. Electronic transport properties of a tilted graphene p-n junction. *Phys. Rev. B* **80**, 155406 (2009).
[5] Wallace, P. R. The Band Theory of Graphite. *Phys. Rev.* **71**, 622-634 (1947).
[6] S. Datta, Electronic Transport in Mesoscopic System, Cambridge University Press (1997).
[7] M. Di Ventra, Electrical Transport in Nanoscale System, Cambridge University Press (2008).
[8] Sancho, M. P. L., Sancho, J. M. L., & Rubio, J. Quick iterative scheme for the calculation of transfer matrices: application to Mo (100). *J. Phys. F: Met. Phys.* **14**, 1205

DOI: 10.1038/NNANO.2011.3

(1984).
[9] Guinea, F., Tejedor, C., Flores, F., & Louis, E. Effective two-dimensional Hamiltonian at surfaces. *Phys. Rev. B* **28**, 4397 (1983).
[10] Anantram, M. P., Lundstrom, M. S., & Nikonov, D. E. Modeling of Nanoscale Devices. *Proc. IEEE* **96**, 1511 (2008).
[11] Grosso, G., Moroni S., & Parravicini, G. P. Electronic structure of the InAs-GaSb superlattice studied by the renormalization method. *Phys. Rev. B* **40**, 12328 (1989).
[12] Low T. Ballistic-Ohmic quantum Hall plateau transition in a graphene p-n junction. *Phys. Rev. B* **80**, 205423 (2009).